Inorganic Chemistry

Article

pubs.acs.org/IC

Solvothermal Synthesis of NiCo Alloy Icosahedral Nanocrystals

Mingzhu Cheng, Ming Wen,* Shiqing Zhou, Qingsheng Wu,* and Baolei Sun

Department of Chemistry, Tongji University, Shanghai 200092, The People's Republic of China

Supporting Information

ABSTRACT: New dimensional NiCo alloy icosahedral nanocrystals with controllable size have been first reported and synthesized through an Ostwald ripening process in a template-absent solvothermal reaction system. The proposed synthesis is corroborated by scanning electron microscopy (SEM), transmission electron microscopy (TEM), X-ray diffraction analysis (XRD), energy-dispersive X-ray spectroscopy (EDX), and X-ray photoelectron spectroscopy (XPS). The as-obtained NiCo icosahedral nanocrystals exhibit the size- and component-dependent magnetic behaviors. The coercivity (H_c) depends on both the magnetocrystalline and structure anisotropy, and the saturation magnetizations (M_s) decided by the content of Co. H_c decreases from 189.02 to 147.95 Oe with the increase of the icosahedral NCs size from 200 to 850 nm. Especially, the H_c of the icosahedral NCs at 157.38 Oe is higher than that of nanospheres at 104.02 Oe. In addition, M_s and H_c increased with the increasing Co content. It can be an ideal building block for applications in magnetic media, sensors, and other devices.

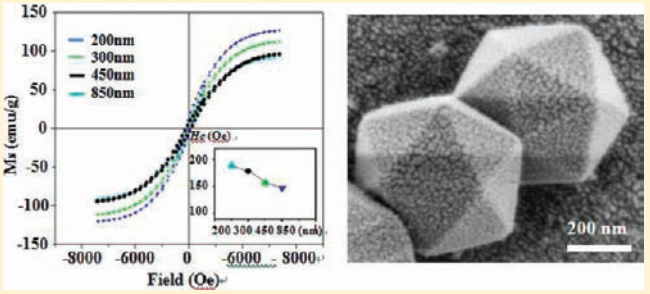

1. INTRODUCTION

Uniform polyhedral nanocrystals (NCs) have attracted remarkable attention because their catalytic, electrical, and magnetic performance can be finely tuned either by their composition, which mediates electron structure, or their shapes, which determine surface atomic arrangement and coordination.[1−8] Because the surface structure changes as a function of size, shape, and number of components of a particle,[9] and the large particle surface area results in increased interaction with their environment, these effects may lead to a radical alteration in chemical reactivity. Therefore, the reactivity and selectivity of catalysts greatly depend upon the arrangement of surface atoms and the number of dangling bonds on the crystal planes. For the purpose of higher catalytic activity, the polyhedron with uniform nanocrystal plane is expected to be prepared due to the different kinds of active sites with different reactivity for different exposed crystal planes, since the different exposed crystal planes have different kinds of active sites and present different reactivities.[10,11]

Recently, most of the reported investigations concerned the noble metal NCs, such as Pt tetrahexahedrons;[10] Au−Cu nanocubes;[11] Au−Pd core−shell nanocrystals with tetrahexahedral, concave octahedral, and octahedral structures;[12] and so on, which are synthesized by solvothermal routes and electrochemical treatment within template direction. However, it is a large challenge to obtain shape- and size-controlled magnetic noble-metal-free alloy polyhedral NCs with better productivity, in spite of the tunable composition and shape which have technological applications including magnetic carriers, biosensors, and bioseparation.[13,14] Until now, few reports are known about magnetic NiCo alloy NCs with icosahedral shape although there are some template-assisted NiCo nanoparticles.[15] In our continuous efforts to improve the synthesis of magnetic nanoalloys,[16] we herein first report on the one-step template-absent synthesis of uniform magnetic NiCo alloy icosahedral NCs ranging in size from 200 to 850 nm in solvothermal reaction system. To the best of our knowledge, it is a very rare case to obtain icosahedral NCs in a NiCo alloy system, especially generated by a solvothermal chemistry reaction, and this facile method can easily suggest the large industrial production in contrast to the electrochemical treatment.

In this work, new dimensional NiCo alloy icosahedral NCs with controllable size and magnetism are synthesized in a solvothermal template-absent system through an Ostwald ripening process. The morphology, structure, formation mechanism, magnetic property, and relativity have been investigated. The measurement results show that magnetic behavior is dependent on size and component, in which coercivity (H_c) decreases with increasing icosahedral NC size. In addition, saturation magnetization (M_s) and H_c increased with increasing Co content. This new dimensional NiCo alloy icosahedral NC can be an ideal building block for applications in magnetic carriers, sensors, and other devices.

2. EXPERIMENTAL SECTION

2.1. Chemicals. All the reagents used in this work, including nickel(II) acetate hydrate ($Ni(Ac)_2{\cdot}4H_2O$, 99%), cobalt(II) acetate hydrate ($Co(Ac)_2{\cdot}4H_2O$, 99%), sodium hydroxide (NaOH, 99%), polyvinyl pyrrolidone (PVP, average molecular weight is 30 000), absolute ethyl alcohol (C_2H_5OH, 99%), and propylene glycol

Received: August 13, 2011
Published: January 18, 2012

($C_3H_8O_2$, 99%), were purchased from Sinopharm Chemical Reagent Co., Ltd., and were used without further purification.

2.2. Synthesis. NiCo icosahedra nanocrystals were synthesized through an Ostwald ripening process in a solvothermal system. $Ni(Ac)_2{\cdot}4H_2O$, $Co(Ac)_2{\cdot}4H_2O$, NaOH, and PVP were used as precursors. As an example of a typical process, the synthesis process of $Ni_{48}Co_{52}$ icosahedral nanocrystals was described as follows: 3 mL of ethyl alcohol was mixed with 0.06 mmol $Ni(Ac)_2{\cdot}4H_2O$, 0.06 mmol $Co(Ac)_2{\cdot}4H_2O$, 1.2 mmol NaOH, and 0.24 mmol PVP at room temperature. The mixture was dissolved by ultrasonic decomposition. Then, 7 mL of propylene glycol was injected into this mixture and transferred to the autoclave in room temperature. The autoclave was sealed and maintained at 210 °C for 6 h. After the reaction was cooled to room temperature, the NiCo icosahedral nanocrystals were collected at the bottom of the container. The products were alternately washed by distilled water and ethanol with centrifugation thrice, and then were redispersed and stored in ethanol. In addition, the series of NiCo nanoalloys were prepared using the initial molar ratios of Ni^{2+}:Co^{2+} at 100:0, 83:17, 75:25, 50:50, 25:75, 17:83, and 0:100, for the component of Ni, $Ni_{82}Co_{18}$, $Ni_{76}Co_{24}$, $Ni_{48}Co_{52}$, $Ni_{25}Co_{75}$, $Ni_{16}Co_{84}$, and Co, respectively. Detailed data of as-obtained nanoalloy components and their magnetic parameters are summarized in Table S1.

2.3. Atomic Absorption Experiments. Atomic absorption experiments are used to confirm the elemental percentages. The detail experiment is carried out as follows. The as-obtained NiCo nanocrystals were freeze-dried overnight. A 1.25 mg sample of dried NiCo nanoalloy was recovered after ensuring that they were completely dry. Then, 2 mL of aqua regia was added to the vial to digest the serials of NiCo nanoalloys. The resulting solution was heated to ~50 °C for 3 h. The solution turned from a light yellow to a bright neon green. After digestion, the solution was allowed to cool down and was diluted down with deionized water to the appropriate concentration for atomic absorption experiments. The results show that NiCo nanoalloys contain (by weight) 100% Ni for Ni(S1); 81% of Ni and 19% of Co for $Ni_{82}Co_{18}$ (S2); 72% of Ni and 28% of Co for $Ni_{76}Co_{24}$ (S3); 45% of Ni and 55% of Co for $Ni_{48}Co_{52}$ (S4); 23% of Ni and 77% of Co for $Ni_{25}Co_{75}$ (S5); 15% of Ni and 85% of Co for $Ni_{16}Co_{84}$ (S6); 100% of Co for Co (S7), respectively. The contents of Ni and Co are basically consistent with the initial molar ratios between Ni^{2+} and Co^{2+}.

2.4. Characterization. The morphology and size of as-synthesized samples were determined by using Hitachi S-4800 scanning electron microscopy (FE-SEM), JEOL JEM-1200EX (Japan) transmission electron microscopy (TEM), and high resolution transmission electron microscopy (HRTEM). Scanning transmission electron microscopy (STEM) and elemental maps were carried out under the bright field (BF) mode on JEOL JEM-2100 F microscope. Selected area energy dispersive X-ray spectroscopy (EDXS) was conducted at 20 keV on a TN5400 EDS instrument (Oxiford), and all samples were handled under air atmosphere. Powder element analyses of Ni and Co were measured at λ = 232.0 and 240.7 nm by graphite furnace atomic absorption spectrometer (AAS) (6810, Shanghai Chromatogram Technology Company, China). The powder X-ray diffraction (XRD) analysis patterns were recorded using Bruker D8 (German) diffractometer with a Cu Kα X-ray radiation source (λ = 0.154 056 nm). X-ray photoelectron spectroscopy (XPS) experiments were carried out on a RBD upgraded PHI-5000C ESCA system (Perkin-Elmer) with Al Kα radiation (hν = 1486.6 eV). The whole spectra (0–1100 eV) and the narrow spectra of all the elements with much high resolution were both recorded by using RBD 147 interface (RBD Enterprises) through the AugerScan 3.21 software. Binding energies were calibrated by using the containment carbon (C1s = 284.6 eV). The data analysis was carried out by using the RBD AugerScan 3.21 software provided by RBD Enterprises or XPSPeak4.1 provided by Raymund W. M. Kwok (The Chinese University of Hongkong, China). Vibration sample magnetometry (VSM) was used to examine the magnetic properties of as-obtained NiCo nanocrystals on Lakeshore7312.

3. RESULTS AND DISCUSSION

3.1. Synthesis and Characterization of Icosahedral NiCo Nanocrystals. The formation of NiCo icosahedral NCs is carried out through the reduction of Co^{2+} and Ni^{2+} by ethylene glycol in a solvothermal template-absent system. The formation reaction underneath can be suggested as follows.[17] In the present basic reaction condition (pH = 11.5), Co^{2+} and Ni^{2+} become the stable intermediate phase of $Co(OH)_2$ and $Ni(OH)_2$, which is a storehouse of Co^{2+} and Ni^{2+}, and can control the reaction process through the controlling of the release of Co^{2+} and Ni^{2+} in solution.

$$Ni(OH)_2(s) + 2e^- = Ni + 2OH^-(aq)$$
$$\phi^{\theta}_{Ni(OH)_2/Ni} = -0.72\ (V) \quad (1)$$

$$Co(OH)_2(s) + 2e^- = Co + 2OH^-(aq)$$
$$\phi^{\theta}_{Co(OH)_2/Co} = -0.73\ (V) \quad (2)$$

On the basis of the Nernst function, at pH = 11.5 this equation follows:

$$\phi_{Ni(OH)_2/Ni} = \phi^{\theta}_{Ni(OH)_2/Ni} + \frac{0.059}{2}\log\left[\frac{1}{OH}\right]^2$$
$$= -0.72 - 0.059(14 - pH)$$
$$= -0.72 - 0.059(14 - 11.5)$$
$$= -0.5725\ (V)$$

Simultaneously

$$\phi_{Co(OH)_2/Co} = -0.5825\ (V)$$

On the other hand, as reducer

$$C_2O_4^{2-}(aq) + 8H_2O(1) + 8e^- = C_2H_6O_2(1) + 10OH^-(aq)$$
$$\phi^{\theta}_{C_2O_4^{2-}/C_2H_6O_2} = -0.91\ (V) \quad (3)$$

When pH = 11.5

$$\phi_{C_2O_4^{2-}/C_2H_6O_2} = \phi^{\theta}_{C_2O_4^{2-}/C_2H_6O_2} + \frac{0.059}{8}\log\left[\frac{1}{OH}\right]^{10}$$
$$= -0.91 + 0.074(14 - pH)$$
$$= -0.91 + 0.074(14 - 11.5)$$
$$= -0.725\ (V)$$

Further oxidation gives

$$2CO_3^{2-}(aq) + 2H_2O(l) + 2e^- = C_2O_4^{2-}(aq) + 4OH^-(aq)$$
$$\phi^{\theta}_{CO_3^{2-}/C_2O_4^{2-}} = -1.05\ (V) \quad (4)$$

dx.doi.org/10.1021/ic201763j | Inorg. Chem. 2012, 51, 1495–1500

When pH = 11.5

$$\phi_{CO_3^{2-}/C_2O_4^{2-}} = \phi^{\theta}_{CO_3^{2-}/C_2O_4^{2-}} + \frac{0.059}{2}\log\left[\frac{1}{OH}\right]^4$$

$$= -1.05 + 0.118(14 - pH)$$

$$= -1.05 + 0.118(14 - 11.5)$$

$$= -0.755\ (V)$$

So

$$\phi_{Ni(OH)_2/Ni},\ \phi_{Co(OH)_2/Co} > \phi_{C_2O_4^{2-}/C_2H_6O_2} > \phi_{C_2O_4^{2-}/C_2H_6O_2}$$

Thus, the reaction is carried out following reaction (4). Ethylene glycol finally completely is oxidized forming CO_3^{2-}. Therefore, Co^{2+} and Ni^{2+} can be completely reduced by ethylene glycol under present conditions. The total reaction function is given as follows:

$$C_2H_6O_2(1) + 5Ni(OH)_2(s) + 4OH^- = 2CO_3^{2-} + 5Ni(s) + 10H_2O(1)$$

$$3C_2H_6O_2(1) + 10Co(OH)_3(s) + 12OH^- = 6CO_3^{2-} + 10Co(s) + 30H_2O(1)$$

The morphology of as-synthesized NiCo alloy icosahedral NCs was determined initially by FE-SEM, and shown in Figure 1a. The average size of icosahedral NiCo NCs was ~450 nm with a yield of ~65%. A high magnification SEM image of icosahedral NiCo NCs oriented along the 5-fold axes is presented in inset I of Figure 1a. The icosahedral shape is bounded by 20 regular triangle facets and 12 vertices, in which each vertex was formed by five triangle planes with two adjecent facets angles of 138.19°.[18] In some cases, shown in inset II of Figure 1a, imperfection can be introduced at vertices, which is not caused by the {220} truncation of icosahedral NC but rather because crystal facets of different sizes are produced by substrate effects. TEM analysis in bright-field (Figure 1c) and dark-field (Figure 1d) indicates that such structure clearly reveals three-dimensional (3D) structure of the NCs. The regular hexagon with observed inner angle of 120° for a single icosahedral NiCo NC in Figure 1c under TEM confirms the 3D icosohedron shape. The facets of the icosahedral NiCo NCs were determined by HRTEM and selected-area electron diffraction (SAED) pattern. Figure 1b presents HRTEM image recorded from a boxed area I marked in Figure 1c. The dominant exposed facets of the NiCo icosahedral NCs are {112}, which are the only plane normal to both the plane of (111) with a lattice space of 0.21 nm and the plane of (220) with a crossing lattice space of 0.13 nm. The SAED recorded from boxed areas I and II marked in Figure 1c are given in the insets of Figure 1e,f, respectively. The 3-fold symmetry of the SAED pattern confirms that the icosahedral NiCo NC is a single crystal, and can be indexed as (111) and (220) planes. Figure 2a–c shows representative STEM images and the corresponding EDXS maps for Ni and Co in a single icosahedral NC, indicating icosahedral NC is a NiCo alloy. EDXS performed on NiCo alloy icosahedral NCs undoubtedly indicates that they contain Ni and Co with the ratio of ~1/1 in Figure 2d. The composition analysis for other NiCo NCs are

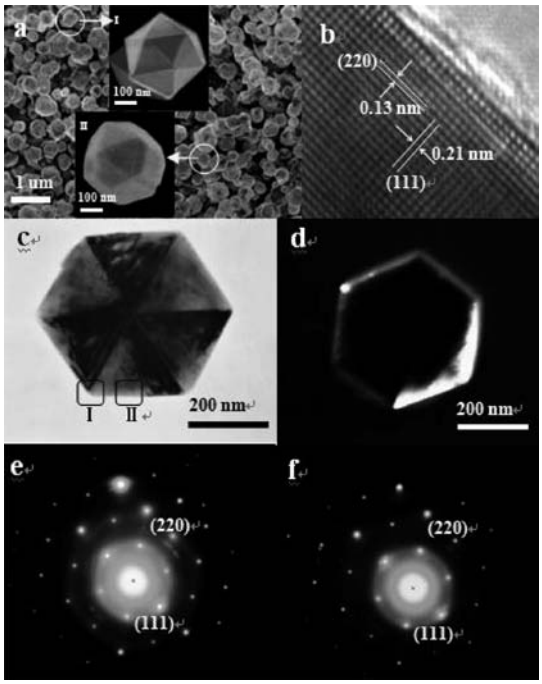

Figure 1. (a) SEM image of icosahedral NiCo NCs with inset high-magnification images of a perfect (I) and an imperfect (II) icosahedral NC. (b) HRTEM image recorded from the boxed area I marked in part f. (c) Bright-field and (d) dark-field TEM image of a single icosahedral NiCo NC. (e, f) Corresponding SAED pattern recordered from the boxed area I and II marked in part f, respectively.

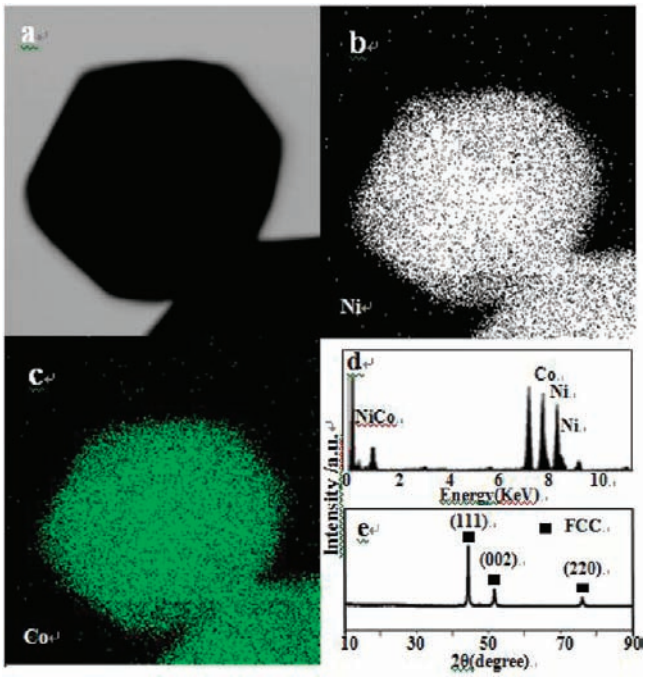

Figure 2. (a) BF-STEM image of a icosahedral NiCo NC. (b) XRD pattern of icosahedral NiCo NCs. (c) EDXS of NiCo icosahedral NCs. (d, e) The elemental maps of Ni and Co in a icosahedral NiCo NC, respectively.

dx.doi.org/10.1021/ic201763j | Inorg. Chem. 2012, 51, 1495–1500

confirmed by AAS and EDXS (Supporting Information, Table S1 and Figure S1). In Figure 3, the XRD pattern of NiCo

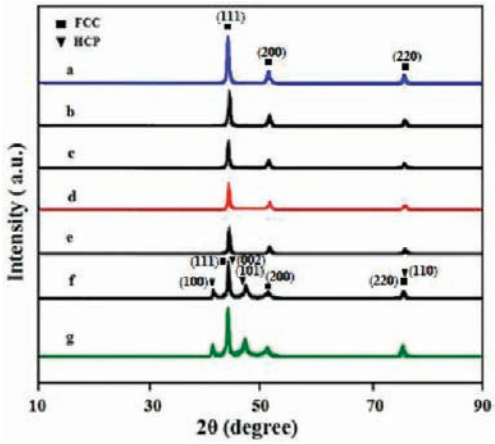

Figure 3. XRD patterns of NiCo nanocrystals in different compositions: (a) Ni, (b) $Ni_{82}Co_{18}$, (c) $Ni_{76}Co_{24}$, (d) $Ni_{48}Co_{52}$, (e) $Ni_{25}Co_{75}$, (f) $Ni_{16}Co_{84}$, (g) Co.

icosahedral NCs is similar to those of either Ni or Co with an fcc structure (JCPDS 01-1260 and 15-0806) and corresponding to (111) and (220) in SAED pattern in Figure 1e,f, while the content of Co over 84 at. % in NiCo NCs results in the mixed structures of hcp and fcc.[19,20] The growth process of NiCo alloy icosahedral NCs was monitored by withdrawing samples at different growth periods in Figure S2 in Supporting Information. During the early stages, Ni^{2+} and Co^{2+} were reduced by propylene glycol and alloyed to the aggregation of NiCo alloy nucleus. In the current reaction system, the nanocrystal morphology tends to be dictated by underlying crystal structure, and the NiCo alloy nucleus then formed small icosahedral NCs because Ni−Co alloy clusters have an icosahedral morphology.[21,22] The further growth gives large perfect icosahedral NCs with edge-shapening and size-focusing by Ostwald ripening.[23,24] Finally, the growth leads to the presentation of bounded facets of {112} as the time prolongs to 6 h. After 10 h, the morphology remained similar to that at 6 h with relatively larger size. Thus, the formation of icosahedral NCs can be completed at ∼6 h. Scheme S1 in Supporting Information shows the representative surface atom arrangement of the fcc NiCo icosahedral NCs with different crystal planes. The area of adjacent four atoms of the {111} (b), {220} (c), and {112} (d) facets is $(\sqrt{3}/2)\alpha^2$, $(\sqrt{2}/2)\alpha^2$, and $(\sqrt{6}/2)\alpha^2$, respectively, suggesting the {112} planes are more open than the {111} and {220} planes. Of the three planes, the most densely packed {111} planes have the lowest surface energy based on its surface atoms having the smallest number of missing nearest neighbors per unit area. Therefore, the {112} planes have a more reactive surface.

In Figure 4, X-ray photoelectron spectroscopy (XPS) shows five photoemission peaks for Ni2p, Co2p, C1s, and O1s. Magnified Ni2p peaks, consisting of two peaks at 851.8 and 870.7 eV, are due to the spin−orbit splitting of $2p_{3/2}$ and $2p_{1/2}$, indicating dominant Ni(0). For Co2p, two peaks resulting from the 2p electron multiplet-splitting are $2p_{3/2}$ and $2p_{1/2}$ with the binding energy of 779.15 and 794.18 eV, implying Co(0). In *Binding Energy Lookup Table for Signals from Elements and Common Chemical Species*, C1s = 285.0, $Co2p_{3/2}$ = 778.3, $Co2p_{1/2}$ = 793.7, $Ni2p_{3/2}$ = 852.6, $Ni2p_{1/2}$ = 869.9, respectively.

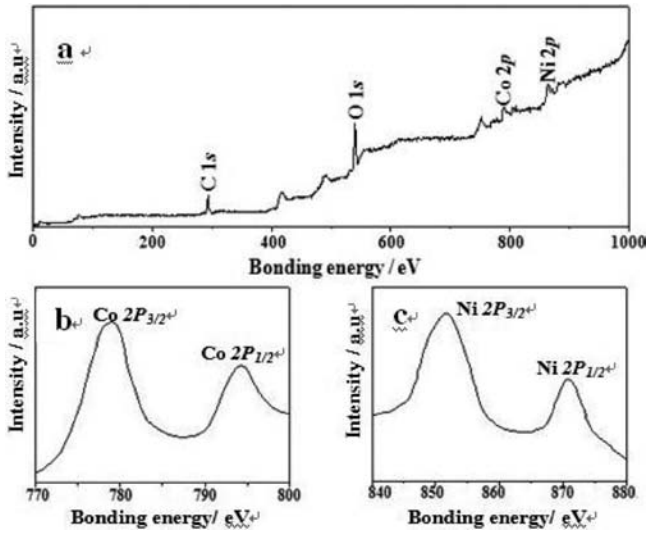

Figure 4. (a) XPS spectra for NiCo icosohedral nanocrystals. (b) Detailed spectra of Co2p. (c) Detailed spectra of Ni2p. All the horizontal axes represent the binding energy corrected by that of C1s.

Owing to the different environments, the signals of metallic bonding energy in as-obtained NiCo alloy NCs are slightly shifted compared with the pure nickel and cobalt bulk metals.

The shape of NiCo NCs could be controlled by varying the composition and the reaction conditions based on the growth habit (which is leaded by the underlying crystal structure). In Figure 5, owing to the influence of the growth habits of Ni and Co, with increasing Co content, the shape changes from multihorn-sphere in Ni and $Ni_{82}Co_{18}$ to icosahedral NCs in $Ni_{48}Co_{52}$, and then to hexagonal plate in $Ni_{16}Co_{84}$. In addition, the molar ratio of NaOH:M^{2+} and PVP:M^{2+} in the reaction system is the important effect factor of the shape of NiCo nanoalloys. The clear icosohedral shape with uniform size of about ∼450 nm can be observed when the molar ratio of NaOH:M^{2+} is 1:10 (Surpporting Information, Figure S3) and of PVP:M^{2+} is 1:2 (Surpporting Information, Figure S4). The size of the icosahedral NiCo NCs can be adjusted by the concentration of the metal precursor at the above optimized concentration of NaOH and PVP. The SEM images of NiCo icosahedral NCs obtained in the concentration of M^{2+} at 4, 6, 8, and 10 mM are shown in Figure 6. The corresponding average sizes are ∼200, ∼ 300, ∼ 450, and ∼850 nm, respectively.

3.2. Magnetic Properties of NiCo Nanoalloys. Hysteresis measurement results show that the magnetic behavior is dependent on the size and component. Figure 7a shows the magnetic behavior of the icosahedral NCs in different sizes measured at 300 K, and the detailed data are summarized in Table S2 in Supporting Information. Generally, as the particle size increases, the coercivity (H_c) increases rapidly upon the size exceeding the superparamagnetic limit, saturates when the size approaches the single-domain limit, and gradually decreases to the bulk value upon passing the multidomain region (Supporting Information, Figure S5).[25] Because the reported single-domain limit of 20 and 32 nm was estimated for Co and Ni nanoparticles,[26] our icosahedral NiCo NCs show H_c decreases from 189.02 to 147.95 Oe with the size increase from 200 to 850 nm because of their size all over the single-domain limit. This variation trend of H_c over size can be clearly observed in the inset of Figure 7a. The different components of NiCo nanoalloys within the different shapes from multihorn-

dx.doi.org/10.1021/ic201763j | Inorg. Chem. 2012, 51, 1495−1500

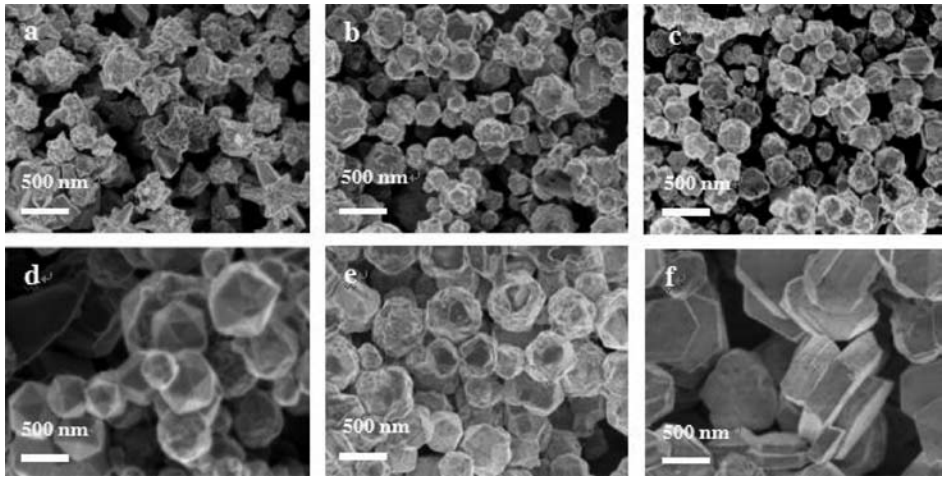

Figure 5. SEM images of NiCo NCs in different compositions: (a, b) Ni and $Ni_{82}Co_{18}$ multihorn-sphere, (c) $Ni_{76}Co_{24}$ irregular polyhedral NCs, (d) $Ni_{48}Co_{52}$ icosahedral NCs, (e) $Ni_{25}Co_{75}$ truncation icosahedral NCs, (f) $Ni_{16}Co_{84}$ nanoplates.

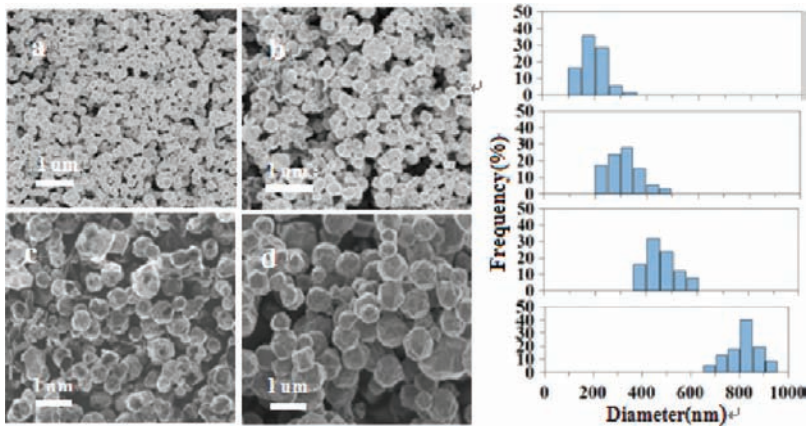

Figure 6. SEM images of icosahedral NiCo NCs within different sizes: (a) ~200 nm, (b) ~300 nm, (c) ~450 nm, (d) ~850 nm. (e) Size distributions of icosahedral NiCo NCs in parts a–d, respectively, after counting more than 200 particles for each sample.

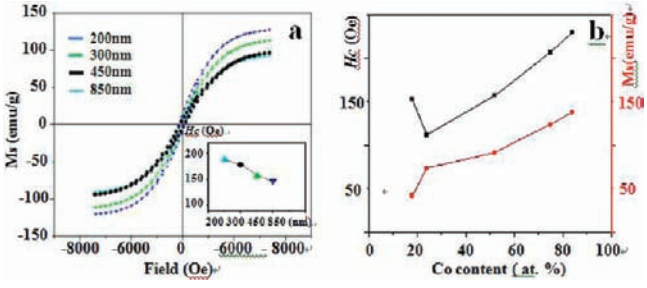

Figure 7. Magnetic behavior of icosahedral NiCo NCs measured at 300 K: (a) M–H curves for 200, 300, 450, and 850 nm sized icosahedral NCs with inset curve of H_c over the particle size. (b) The variation of M_s and H_c for NiCo NCs within different compositions.

sphere to icosahedron and then to plate exhibit different magnetic properties; the values of M_s and H_c over the content of Co are plotted in Figure 7b. The increase of Co content resulted in an increase of M_s from 42 to 139 emu/g, induced by the difference of atomic magnetic dipole moment between Ni (0.6 μ_B) and Co atoms (1.75 μ_B).[27] However, H_c depends on effective anisotropy which is decided by both the magneto-crystalline and shape anisotropy. For fcc structure, the magnetocrystalline anisotropy constant K_1 of Co is higher than that of Ni. So, H_c increases with increasing Co content, and together with the effect of shape anisotropy lead to the variation trend in Figure 7b. The detailed data are summarized in Table S1 in Supporting Information.

4. CONCLUSION

In conclusion, we have reported here new dimensional NiCo alloy icosahedral NCs with controllable size and magnetism synthesized through an Ostwald Ripening process. The as-synthesized icosahedral NCs of NiCo nanoalloys are bounded by the active predominantly exposed planes of {112}. The magnetic properties of NiCo alloy NCs indicated that the magnetic behavior is dependent on size, shape, and composition. H_c decreases with the increase of icosahedral NC size. In addition, the Co content increase can increase the M_s and H_c of as-obtained NiCo nanoalloys. This approach can be readily extended to the synthesis of polyhedron NCs of other related magnetic transition metal alloys without noble metals. The preparation of these magnetic alloy polyhedron NCs with uniform reactive crystal facets is expected to bring up a new way to design and control physical and chemical specificity, suggesting the applications in magnetic carriers, sensors, and other devices.

dx.doi.org/10.1021/ic201763j | Inorg. Chem. 2012, 51, 1495–1500

■ ASSOCIATED CONTENT

Supporting Information

SEM and TEM images, EDX spectroscopy, and the detailed data of alloy composition and magnetic parameters. This material is available free of charge via the Internet at http://pubs.acs.org.

■ AUTHOR INFORMATION

Corresponding Author

*E-mail: m_wen@tongji.edu.cn (M.W.); qswu@tongji.edu.cn (Q.W.). Phone: +86-21-65982653 ext 8544. Fax: +86-21-65981097.

■ ACKNOWLEDGMENTS

This work was financially supported by the National Natural Science Foundation of China (Nos. 21171130, 51072134, and 91122025), Innovation Program of SECF (10ZZ21), and 973 Project of China (No. 2011CB932404).

■ REFERENCES

(1) Zhang, J.; Sasaki, K.; Sutter, E.; Adzic, R. R. *Science* **2007**, *315*, 220−222.
(2) Hu, L. H.; Peng, Q.; Li, Y. D. *J. Am. Chem. Soc.* **2008**, *130*, 16136−16137.
(3) Hu, M. J.; Lu, Y.; Zhang, S.; Guo, S. R.; Lin, B.; Zhang, M.; Yu, S. H. *J. Am. Chem. Soc.* **2008**, *130*, 11606−11607.
(4) Kim, D.; Lee, N.; Park, M.; Hyo Kim, B.; An, K.; Hyeon, T. *J. Am. Chem. Soc.* **2009**, *131*, 454−455.
(5) Hu, M. J.; Lu, Y.; Zhang, S.; Guo, S. R.; Line, B.; Zhang, M.; Yu, S. H. *J. Am. Chem. Soc.* **2008**, *130*, 11606−11607.
(6) Burda, C.; Chen, X.; Narayanan, R.; EI-Sayed, M. A. *Chem. Rev.* **2005**, *105*, 1025−1102.
(7) Zhou, K. B.; Wang, X.; Sun, X. M.; Peng, Q.; Li, Y. D. *J. Catal.* **2005**, *229*, 206−212.
(8) Si, R.; Flytzani-Stephanopoulos, M. *Angew. Chem., Int. Ed.* **2008**, *47*, 2884−2887.
(9) Miguel, J. Y.; Eduardo, P. T.; Sergio, M. R. *J. Mater. Chem.* **2007**, *17*, 1035−1038.
(10) Tian, N.; Zhou, Z. Y.; Sun, S. G.; Ding, Y.; Wang, Z. L. *Science* **2007**, *316*, 732−735.
(11) Liu, Y. L.; Hight Walker, A. R. *Angew. Chem., Int. Ed.* **2010**, *49*, 1−6.
(12) Lu, C. L.; Sudhakara Prasad, K.; Wu, H. L.; Ho, J.-a. A.; Huang, M. H. *J. Am. Chem. Soc.* **2010**, *132*, 14546−14553.
(13) Xie, J.; Chen, K.; Lee, H. Y.; Xu, C.; Hsu, A. R.; Peng, S.; Chen, X.; Sun, S. *J. Am. Chem. Soc.* **2008**, *130*, 7542−7543.
(14) Hu, M. J.; Lu, Y.; Zhang, S.; Guo, S. R.; Line, B.; Zhang, M.; Yu, S. H. *J. Am. Chem. Soc.* **2008**, *130*, 11606−11607.
(15) Lim, S. K.; Ban, K. S.; Kim, Y. H.; Kim, C. K.; Yoon, C. S. *Appl. Phys. Lett.* **2006**, *88*, 163102.
(16) (a) Wen, M.; Yang, D.; Wu, Q. S.; Lu, R. P.; Zhu, Y. Z.; Zhang, F. *Chem. Commun.* **2010**, *46*, 219−221. (b) Wen, M.; Wang, Y. F.; Zhang, F.; Wu, Q. S. *J. Phys. Chem. C* **2009**, *113*, 5960−5966. (c) Zhang, F.; Wen, M.; Cheng, M. Z.; Wu, Q. S. *J. Mater. Chem.* **2010**, *20*, 7661−7668. (d) Wen, M.; Zhang, F.; Cheng, M. Z.; Wu, Q. S.; Sun, B. L.; Sun, Y. Z. *ChemPhysChem* **2011**, *12*, 3573−3577.
(17) Hu, M. J.; Lin, B.; Yu, S. H. *Nano Res.* **2008**, *1*, 302−313.
(18) Billas, I. M.L.; Châtelain, A.; Heer, W. A. D. *Science* **1994**, *265* (5179), 1682−1683.
(19) Liu, Z. P.; Yang, Y.; Peng, S.; Hu, Z. K.; Qian, Y. T. *Adv. Mater.* **2003**, *15*, 936−940.
(20) Mi, Y.; Yuan, D.; Liu, Y.; Zhang, J.; Xiao, Y. T. *Mater. Chem. Phys.* **2005**, *89*, 359−361.
(21) Pellarin, M.; Cottancin, E.; Lermé, J.; Vialle, J. L.; Wolf, J. P.; Broyer, M.; Paillard, V.; Dupuis, V.; Perez, A.; Perez, J. P.; Tuaillon, J.; Melinon, P. *Chem. Phys. Lett.* **1994**, *217*, 349.
(22) Robert, W. G. *Encyclopedia Polyhedra: ICOSAHEDRON* **2007**, *7*, 28.
(23) Seo, D.; Park, J. C.; Song, H. *J. Am. Chem. Soc.* **2006**, *128* (46), 14863−14870.
(24) Hoang, T. K. N.; Deriemaeker, L.; La, V. B.; Finsy, R. *Langmuir* **2004**, *20* (21), 8966−8969.
(25) Klabunde, K. J. *Nanoscale Materials in Chemistry*; Wiley-Interscience: New York, 2001; Vol. 3, pp 263−277.
(26) Gong, W.; Li, H.; Zhao, Z.; Chen, J. *J. Appl. Phys.* **1991**, *69*, 5119−5121.
(27) Dinega, D. P.; Bawendi, M. G. *Angew. Chem., Int. Ed.* **1999**, *38*, 1788−1791.